Article

Study on Multi-Mode Switching Control of Intelligent Suspension under Full Road Section

Zhaole Qu, Jianze Liu * , **Yang Li, Fazhan Yang and Jiang Liu**

Institute of Mechanical and Automotive Engineering, Qingdao University of Technology, Qingdao 266520, China; 18865486725@163.com (Z.Q.); yangli@qut.edu.cn (Y.L.); fazhany@163.com (F.Y.); liujiang@qut.edu.cn (J.L.)
* Correspondence: liujianze@qut.edu.cn; Tel.: +86-15966766092

Abstract: The safety, comfort, and energy feedback of active suspension in a single control mode is mutually restricted. To meet the needs of drivers and passengers for vehicle driving performance under different road conditions, this paper proposes a multi-mode switching control strategy of an intelligent suspension system, aiming at improving the stability and comfort of vehicles under different road conditions. In this paper, the adaptive Kalman filter algorithm with a forgetting factor is used to estimate the road input. The accuracy of the algorithm in estimating the road input is verified by simulation and experiment. The single-double threshold logic judgment method is used to formulate the switching rules between each working mode. In the controller, the PID control of the BP neural network and the LQR control optimized by GA are used to optimize and adjust the vehicle driving performance indexes in different modes, which effectively solves the problem of limited adaptability of suspension control optimization objectives under different road driving conditions. Based on the data from the vehicle acceleration sensor and road condition sensor, the modeling and simulation of the switching control system are carried out. The simulation results show that the designed control system can effectively improve the comprehensive performance of the vehicle under different road driving conditions. Compared with the traditional active suspension, the body acceleration is increased by 26% on the B-grade road surface, which effectively improves the user's ride comfort. Compared with the traditional active suspension, the tire dynamic displacement is increased by 24% on the D-grade road, which can significantly improve the overall performance of the vehicle and meet the design requirements of the system.

Keywords: active suspension; multi-mode switching; adaptive Kalman filtering algorithm; BP-PID control; GA-LQR control

1. Introduction

With the development of society and the improvement in people's living standards, users have put forward higher requirements for the safety and comfort of vehicles. Because the stiffness and damping of the passive suspension are not adjustable, it can only ensure the optimal damping effect under certain circumstances. It is difficult to adapt to different roads and use conditions, and it is difficult to obtain good ride comfort and handling stability at the same time. As an advanced suspension system, the active suspension can switch the corresponding working mode according to the road condition and driving state, and actively adjust the suspension hardness to improve the stability and comfort of the vehicle [1–3]. Therefore, the research on multi-mode switching control strategies for active suspension has become one of the hotspots in the field of automobile engineering.

Researchers have conducted extensive studies on the multi-mode switching control strategy of automobile suspension and have achieved certain results. Tang Shichen et al. [4] took the vehicle full active suspension system with three parallel damping adjustable shock absorbers as the research object and designed three damping working modes of 'soft', 'medium', and 'hard', respectively. The switching control rules between damping

working modes were determined according to the actual driving conditions of the vehicle. On this basis, according to the suspension performance indexes under different damping working modes, the optimal controllers of active suspension are designed respectively. Wang et al. [5] used the finite state machine (FSM) as the theoretical basis to establish a switching control system. Based on the model reference adaptive control method, the adaptive control part was improved to adaptive mode switching, and the hybrid suspension was multi-mode switching control. On this basis, the passive reference suspension model is used to provide real-time vehicle reference performance indicators. By comparing with the switching conditions, the hybrid suspension is controlled to adjust the control method in four different modes to achieve adaptive adjustment. Liu et al. [6] identified the type of road surface by collecting road image data and using a convolutional neural network (CNN). They used the genetic optimization algorithm to find the optimal parameters of a semi-active suspension system under different road surfaces and realized the adaptive adjustment of suspension control parameters under different road surfaces according to the road surface recognition results [7,8].

Although the above methods can effectively identify different road conditions and switch effectively in different road modes, there are two problems in the multi-mode switching control strategy studied by the above scholars. On the one hand, the above scholars studied and designed the adaptive switching strategy of active suspension, which did not fully consider the driver's independent choice and ignored the driver's demand for vehicle suspension performance. Secondly, in the above multi-mode switching control strategy research, the active suspension controller adopts a single control algorithm, which is easy to cause the problem that the adaptability of the suspension control optimization target of the vehicle under different road driving conditions is limited. For example, when the car is driving on a B-grade road surface, at this time, due to the small road roughness, we take the ride comfort of the driver and passenger as the main optimization target. The BP-PID control algorithm can be used to effectively improve the ride comfort of the driver when the vehicle is running; however, when the vehicle travels to a road grade with large road roughness, such as a D-grade road surface, if the same BP-PID control algorithm is still used, the optimal control effect may not be achieved, and the vehicle performance index may even deteriorate.

For the Kalman filter estimation of active suspension, Nguyen [9] designed an active suspension controller based on the Kalman filter state estimator and skyhook control algorithm. The linear Kalman filter is used to estimate the required state variables, and the first-order zero-crossing algorithm is used to estimate the road disturbance frequency, which greatly improves the comprehensive performance of the suspension under road disturbance in all frequency regions. Based on the linear model of active hydraulic suspension, Iraj [10] used the extended Kalman filter with Taylor series expansion to realize the nonlinear optimal control of active suspension through suspension state prediction and local residual calculation. Chen et al. [11] designed a 1/4 vehicle Kalman filter and LQG active suspension controller. According to the observation information of three suspension performance observers, the vehicle system uses a linear Kalman filter to estimate the five state variables of the 1/4 vehicle suspension system in real-time to obtain the residuals of each state. After comparing with the set residual thresholds, the error time of the active suspension actuator is obtained in time, and the active control and error self-diagnosis of the active suspension is realized. Through differential geometry analysis and coordinate transformation, Chen et al. [12] simplified the nonlinear suspension vibration model into an observable standard form and combined it with a linear Kalman filter to complete the state estimation and vibration control of the nonlinear suspension.

Although in the above research, scholars can complete more accurate filtering estimation and improve the vibration control of suspension, there is also a third problem that this paper wants to solve, that is, in the above research, the filtering estimation of the active suspension state is realized by the linear Kalman filter. Although this method greatly improves the actual control effect of the active suspension, the process noise variance matrix and the

observation noise variance matrix of the linear filter are both fixed matrices determined by the principle of mathematical statistics [13–16]. However, the process noise variance matrix and the observation noise variance matrix of the suspension system in the actual working conditions are real-time changes, so the filtering estimation of the suspension system state still has errors [11].

Aiming at the above three problems, this paper proposes a sensor-based intelligent suspension system and designs the working mode and its switching strategy, and the underlying controller. The system can adjust the hardness of the suspension in real time by sensing the sensor data of the vehicle and road conditions and has good adaptability and stability. The intelligent suspension system designed in this paper includes four working modes, namely energy feedback, comfort, safety, and comprehensive working mode. The energy-regenerative working mode can ensure that the vehicle can recover and store the energy generated by the vertical vibration of the vehicle suspension when driving on the road with less road roughness, which is used for the range extension of the electric vehicle. The three active control modes can improve the ride comfort, safety, and stability of the vehicle on different roads, and improve the driving performance of the vehicle. In this paper, a single-double threshold working mode switching strategy and corresponding switching threshold are designed based on different grades of pavement, so that the four working modes accurately correspond to the A–D grade pavement. When the pavement grade changes, the intelligent suspension system will recommend the corresponding working mode to the driver through the vehicle application. The driver can switch the working mode according to his own needs. The intelligent suspension respects the driver's independent choice, which can meet the driver's different needs for vehicle performance under different road conditions and improve the driving performance of the vehicle under different road conditions.

In the design of the underlying controller, to solve the problem that the control effect of a single control algorithm is not ideal under different road conditions and the adaptability of the suspension control optimization target is limited, this paper uses different composite control algorithms in three active control working modes to optimize the performance index of the vehicle. For the comfort working mode, to improve the ride comfort of the car when driving on the B-grade road surface, body acceleration is selected as the optimization target. Because the PID controller has the advantages of simple structure, easy adjustment, and fast response, and the BP neural network algorithm has the advantages of strong self-learning and function approximation ability, combined with the advantages of the two, a composite control algorithm is proposed. The BP-PID algorithm is used to design the intelligent suspension comfort controller, and the simulation results show that the controller can effectively reduce the body acceleration amplitude. For the comprehensive working mode, to improve the comprehensive performance of the vehicle driving on the D-grade road surface, the optimal control algorithm is used to design the intelligent suspension bottom comprehensive controller. In the LQR controller, the control effects obtained by using different weighting coefficients are very different. Therefore, the genetic algorithm is used to solve the weighting coefficients, and the superiority of the GA-LQR algorithm is proved by simulation, which can effectively improve the overall performance of the vehicle.

Aiming at the problem that the filter estimation of the suspension state using the linear Kalman filter still has errors, this paper applies the adaptive Kalman filter with forgetting factor in the intelligent suspension system and uses the body acceleration and suspension dynamic stroke as the reference parameters of the filter to identify the road surface of the vehicle. The accuracy of vehicle road surface recognition is verified by experimental equipment, which also provides a theoretical basis for the setting of the corresponding switching threshold of the single-double threshold mode switching strategy.

2. Establishment of an Intelligent Suspension Model

2.1. Establishment of the Random Road Input Model

In this paper, the filtered white noise method of the time domain random road excitation model is used to establish the road input model [17], that is:

$$\dot{z}_n(t) = -2\pi f_0 z_n(t) + 2\pi n_0 \sqrt{G_q(n_0)v_0} W(t) \tag{1}$$

where $z_n(t)$ is the time domain signal of the road spectrum; f_0 is the lower cut-off frequency; $G_q(n_0)$ is the road roughness coefficient; v_0 is the speed; $W(t)$ is the time domain signal of standard Gaussian white noise; n_0 is the reference spatial frequency.

According to the ISO/TC108/SC2N67 and GB7031 'vehicle vibration input–pavement roughness representation' standard, the range and mean value of the vertical displacement power spectral density $G_q(n_0)$ of different grades are listed as shown in Table 1.

Table 1. Eight different grades of typical road roughness.

Road Grade	$G_q(n_0) \times 10^{-6}(\text{m}^{-1})\ n_0 = 0.1\ \text{m}^{-1}$		
	Lower Limit	Geometric Mean	Upper Limits
A	8	16	32
B	32	64	128
C	128	256	512
D	512	1024	2048
E	2048	4096	8192
F	8192	16,384	32,768
G	32,768	65,536	131,072
H	131,072	262,144	524,288

2.2. Establishment of 2-DOF 1/4 Vehicle System Dynamics Model

Because the two-degrees-of-freedom model can reflect the vertical vibration characteristics of the vehicle, the vehicle ride comfort and road adhesion can be evaluated by the vertical vibration acceleration of the vehicle body and the dynamic displacement of the tire. In the design and development stage of the vehicle suspension system, the modified model can characterize the effect and influence of the suspension system on the vehicle and can be used to analyze the vibration characteristics of the vehicle suspension system. To simplify the model, a two-degrees-of-freedom model of $\frac{1}{4}$ vehicle of the active suspension system is established [18], as shown in Figure 1.
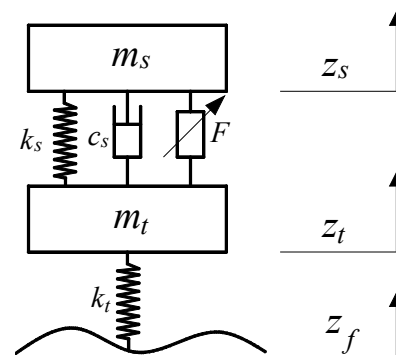

Figure 1. The 1/4 vehicle 2-DOF model.

According to Newton's mechanics, the dynamic equation of the system is:

$$m_s \ddot{z}_s = k_s(z_t - z_s) + c_s(\dot{z}_t - \dot{z}_s) + F \tag{2}$$

$$m_t\ddot{z}_t = k_t\left(z_f - z_t\right) - k_s(z_t - z_s) - F \tag{3}$$

where m_s is the body mass; m_t is the wheel quality; k_s is the suspension spring stiffness; c_s is the suspension damping coefficient; k_t is the tire stiffness; F is the active control force of suspension; z_s is the body displacement; z_t is the suspension displacement; and z_f is pavement displacement.

For the 1/4 vehicle model, body acceleration (BA), suspension working space (SWS), and dynamic wheel displacement (DTD) are the main performance indexes of the vehicle suspension. Therefore, the state variable X and the output variable Y of the suspension system are:

$$X = \begin{bmatrix} \dot{z}_s & \dot{z}_t & z_s & z_t & z_f \end{bmatrix}^T \tag{4}$$

$$Y = \begin{bmatrix} \ddot{z}_s & z_s - z_t & z_t & z_f \end{bmatrix}^T \tag{5}$$

The state space equation of the system is:

$$\begin{cases} \dot{X} = AX + BU + HW \\ Y = CX + DU \end{cases} \tag{6}$$

By writing the system motion equation in matrix form, we can obtain:

$$A = \begin{bmatrix} \frac{-c_s}{m_s} & \frac{c_s}{m_s} & \frac{-k_s}{m_s} & \frac{k_s}{m_s} & 0 \\ \frac{c_s}{m_t} & \frac{-c_s}{m_t} & \frac{k_s}{m_t} & \frac{-k_t-k_s}{m_t} & \frac{k_s}{m_t} \\ 1 & 0 & 0 & 0 & 0 \\ 0 & 1 & 0 & 0 & 0 \\ 0 & 0 & 0 & 0 & -2\pi f_0 \end{bmatrix}; \quad B = \begin{bmatrix} \frac{1}{m_s} \\ \frac{-1}{m_t} \\ 0 \\ 0 \\ 0 \end{bmatrix};$$

$$C = \begin{bmatrix} \frac{-c_s}{m_s} & \frac{c_s}{m_s} & \frac{-k_s}{m_s} & \frac{k_s}{m_s} & 0 \\ 0 & 0 & 1 & -1 & 0 \\ 0 & 0 & 0 & 1 & -1 \end{bmatrix}; \quad D = \begin{bmatrix} \frac{1}{m_s} \\ 0 \\ 0 \end{bmatrix}; \quad H = \begin{bmatrix} 0 \\ 0 \\ 0 \\ 0 \\ 2\pi n_0\sqrt{G(n_0)v_0} \end{bmatrix}.$$

where A is the system matrix, B is the control matrix, C is the output matrix, D is the transfer matrix, H is the road input matrix, $U = F$ is the suspension control force output matrix, and $W = w$ is the Gauss white noise input matrix.

3. Establishment of a Model for Road Grade Estimation Based on Sensors

3.1. Establishment of the Sensor Data Acquisition Model

Acceleration and speed sensors are installed at the body and wheel. The two sensors can measure the motion signals of the body and tire in real time, and the real-time signals are transmitted to the ECU through the analog-to-digital converter. The ECU has a preset working mode switching strategy and a control algorithm designed by different working mode controllers. After the ECU judges and processes the signal, the control signal is transmitted by the digital-to-analog converter. The mode switching signal transmitted to the vehicle application, the user can choose whether to switch the working mode; when the user chooses to switch the working mode, the ball screw actuator is controlled according to the corresponding control algorithm to output the control signal of the DC motor, to improve the performance of the active suspension under different road conditions [19].

To realize the determination of road grade, data acquisition is needed. Therefore, this paper adds sensors, ECUs, energy storage devices, and so on to the traditional suspension system. The specific structure is composed of the parts shown in Figure 2: 1. Body; 2. Spring; 3. Tire; 4. Ground; 5/9. Sensor; 6/8. Analog-to-digital converter; 7. ECU;

10. Suspension damping; 11. Ball screw actuator; 12. Digital-to-analog converter; 13. Energy storage devices.
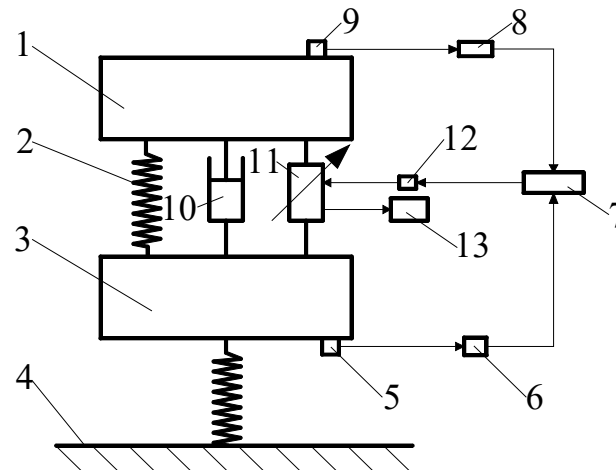

Figure 2. Intelligent suspension structure diagram based on sensor.

3.2. Establishment of the Road Identification Model

At present, there are two main methods to identify road input: the measurement method and filter estimation method based on the filter. The measurement method measures the road surface by setting a road roughness tester or various laser ultrasonic sensors on the vehicle. Although the measured road input accuracy is high and the principle is simple, the measurement equipment is expensive and difficult to apply to the daily vehicle driving process. The filter-based filtering estimation method is based on the vibration response of the vehicle itself when it passes the road surface, and the corresponding road input is obtained through the filter estimation of the filter. The estimation of the road input is more accurate, and the cost is lower.

Therefore, in this paper, the adaptive Kalman filtering algorithm based on genetic factors is used to estimate the road input in the vehicle's active suspension vibration system. Because the Kalman filtering algorithm is easy to program and has few constraints in data processing, it can process the data in the observation period of the system in real time. Therefore, the algorithm has been widely used in many fields such as a vehicle, communication, and navigation control in recent years, and has achieved good estimation results.

3.2.1. Adaptive Kalman Filtering Algorithm

The two-degrees-of-freedom 1/4 vehicle suspension model established above is a continuous differential equation group. Since the Kalman filtering algorithm is a state prediction algorithm, that is, the current state is derived from the previous state, the above differential equations cannot be directly applied to the Kalman filtering algorithm. Before filtering, the system needs to be transformed into a discrete state space equation to describe the dynamic system. Here, the transformation process is no longer deduced in detail, and the discrete state space equation is given directly:

$$\begin{cases} \boldsymbol{X}(t+1) = \boldsymbol{\Phi}\boldsymbol{X}(t) + \boldsymbol{\Gamma}(t)\boldsymbol{W}(t) \\ \boldsymbol{Y}(t) = \boldsymbol{H}\boldsymbol{X}(t) \end{cases} \tag{7}$$

In practical work, the observer will encounter random interference during measurement, and the observed signal usually has observation noise. To make the model more realistic, the observation noise $\boldsymbol{V}(t)$ with the mean value of 0 and variance matrix of $\boldsymbol{R}$ is introduced into the state equation, and the state equation becomes:

$$\begin{cases} \boldsymbol{X}(t+1) = \boldsymbol{\Phi}\boldsymbol{X}(t) + \boldsymbol{\Gamma}(t)\boldsymbol{W}(t) \\ \boldsymbol{Y}(t) = \boldsymbol{H}\boldsymbol{X}(t) + \boldsymbol{V}(t) \end{cases} \tag{8}$$

In the actual movement of the vehicle, the noise variance matrix of the noise measured by the vehicle vibration system observer is not constant but will change with time and road changes, resulting in reduced filtering estimation accuracy [20]. The adaptive Kalman filtering algorithm with the forgetting factor adopted in this paper can not only eliminate the influence of noise change, but also reduce the error of vehicle vibration system modeling, and further filter and estimate the vehicle vibration system to improve the control effect of the system.

This paper starts with the linear Kalman filtering algorithm, and then further introduces the adaptive Kalman filtering algorithm with the forgetting factor. The premise of using Kalman filtering in the discrete space expression of the model shown in Equation (16) is that the noise of the system is uncorrelated white noise with the mean value of 0 and variance matrix of Q and R, respectively [21], and satisfies that the initial state is not related to the observation noise, that is:

$$\begin{cases} \delta_{kk} = 1, \delta_{kj} = 0 \\ E[W(k)] = 0 \\ E[V(k)] = 0 \\ E\left[W(k)W^T(j)\right] = Q\delta_{kj} \\ E\left[V(k)V^T(j)\right] = R\delta_{kj} \\ E[X(0)] = \mu \\ E\left[(X(0) - \mu)(X(0) - \mu)^T\right] = P \end{cases} \tag{9}$$

The principle of linear discrete Kalman filtering is:

(1) The first step is to use the system state of the previous moment to estimate the system state of the present moment:

$$\hat{X}(t + 1|t) = \mathbf{\Phi}(t)\hat{X}(t|t) \tag{10}$$

where $\hat{X}(t|t)$ is the optimal filtering value of the state at the t moment; $\hat{X}(t + 1|t)$ predicts the model state at $t + 1$ the time for the model state at $t + 1$ time.

(2) According to the system error covariance at the previous moment and the process noise variance $Q(t)$ at the $t + 1$ moment, the error covariance at this moment is predicted:

$$P(t + 1|t) = \mathbf{\Phi}(t)P(t|t)\mathbf{\Phi}(t)^T + \mathbf{\Gamma}(t)Q(t)\mathbf{\Gamma}(t)^T \tag{11}$$

where $P(t|t)$ is the error covariance matrix of the system update at t; $P(t + 1|t)$ is the prediction of the error covariance matrix at the $t + 1$ time based on the system state at the time of the t.

(3) The measurement equation is introduced, and the estimated value of $t + 1$ time obtained by Equation (18) is corrected to obtain:

$$\hat{X}(t + 1|t + 1) = \begin{array}{l} \hat{X}(t + 1|t) + K(t + 1|t)\left[Y(t) - C\hat{X}(t + 1|t)\right] \\ \hat{X}(t + 1|t) + K(t + 1|t)\varepsilon(t + 1) \end{array} \tag{12}$$

where $\varepsilon(t) = Y(t) = C\hat{X}(t + 1|t)$ is the difference between the observed value and the predicted value of the filtering state, that is, the measurement margin; $K(t + 1)$ is the Kalman gain coefficient at the $t + 1$ time.

The Kalman gain is related to the output state matrix, the predicted error covariance, and the variance of the observation noise $R(t)$. The expression is as follows:

$$K(t + 1) = \frac{P(t + 1|t)C^T}{CP(t + 1|t)C^T + R(t)} \tag{13}$$

(4) The error covariance matrix is modified to estimate the system state at the time $t + 2$. The expression is:

$$P(t+1|t+1) = [I - K(t+1)C]P(t+1|t) \tag{14}$$

where I is the unit diagonal matrix with the same dimension as the suspension state.

Equations (10)–(14) are the five core formulas of the Kalman filtering algorithm, Equations (10) and (11) are prediction processes, and Equations (12)–(14) are update processes. The schematic diagram is shown in Figure 3.
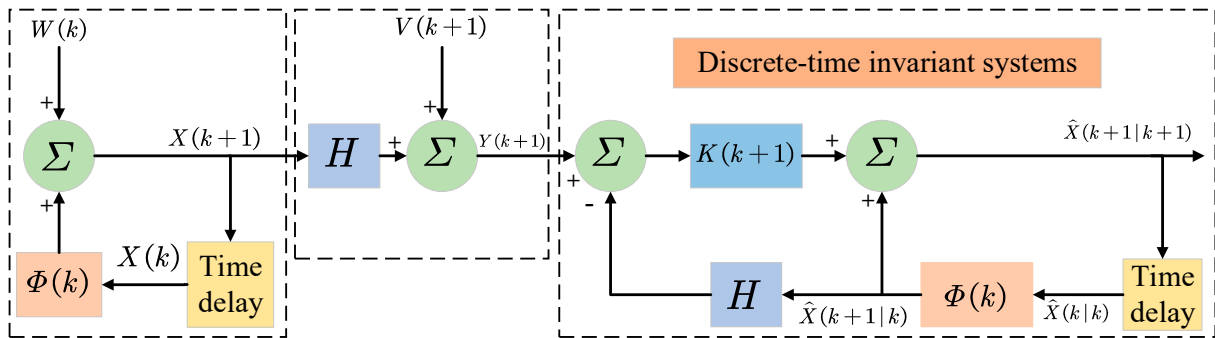

Figure 3. Schematic diagram of the linear discrete Kalman filter.

According to the measurement margin of each step in the filtering process, the adaptive Kalman filtering algorithm corrects the noise variance matrix of the next step by the forgetting factor b and then realizes the filtering estimation of the time-varying noise system. The correction process of the forgetting factor to the time-varying noise variance matrix is:

$$r(t) = (1 - d_t)r(t-1) + d_t[Z(t) - HX(t|t-1)] \tag{15}$$

$$R(t) = (1 - d_t)R(t-1) + d_t\left[\varepsilon(t)\varepsilon^T(t) - HP(t|t-1)H^T\right] \tag{16}$$

where $d_t = \frac{1-b}{1-b^{t+1}}$ is the weighting coefficient of the adaptive Kalman filter, and $0 < b < 1$ is the forgetting factor.

The modified noise variance matrix at each time is substituted into the linear discrete Kalman filter algorithm. The adaptive Kalman filter algorithm equations with a forgetting factor are:

$$\hat{X}(t+1|t) = \mathbf{\Phi}(t)\hat{X}(t|t) \tag{17}$$

$$\hat{P}(t+1|t) = \mathbf{\Phi}P(t|t)\mathbf{\Phi}^T + \mathbf{\Gamma}Q\mathbf{\Gamma}^T \tag{18}$$

$$K(t+1) = \frac{P(t+1|t)H^T}{HP(t+1|t)H^T + R(t+1)} \tag{19}$$

$$\varepsilon(t+1) = Z(t) - H\hat{X}(t+1|t) - r(t) \tag{20}$$

$$\hat{X}(t+1|t+1) = \hat{X}(t|t) + K(t+1)\varepsilon(t+1) \tag{21}$$

$$\hat{P}(t+1|t+1) = [I_n - K(t+1)H]P(t+1|t) \tag{22}$$

When the vehicle passes through the corresponding road surface, due to road roughness and vehicle speed, the road input will be transmitted to the body through the vehicle's active suspension system, so that the body and suspension move up and down with the fluctuation of the road surface. The road input identification filter estimation method is to use the motion of the body and suspension to invert the road input through the filter [22].

It is difficult to directly collect the corresponding data for the tire displacement z_f (the vertical displacement fluctuation at the contact between the tire and the road surface). Therefore, the vehicle speed v_0, the body acceleration $\ddot{z}_s$, and the suspension dynamic stroke $\ddot{z}_s - \ddot{z}_t$ are used as input data. In this paper, the 1/4 suspension model is selected for road identification estimation, and the state variables are the same five-dimensional variables as the formula (5). The measured and highly accurate BA and SWS performance indicators are selected as the observation variables Y of the vehicle road identification model, that is:

$$Y = \begin{bmatrix} \ddot{z}_s \\ \ddot{z}_s - \ddot{z}_t \end{bmatrix} \tag{23}$$

According to the state variable and the observation variable Y, the filtering estimation equations of the system are established as follows:

where $C_p = \begin{bmatrix} \frac{-c_s}{m_s} & \frac{c_s}{m_s} & \frac{-k_s}{m_s} & \frac{k_s}{m_s} & 0 \\ 0 & 1 & 1 & -1 & 0 \end{bmatrix}$; $D_p = \begin{bmatrix} \frac{1}{m_s} \\ 0 \end{bmatrix}$.

Substituting the above formula into the adaptive Kalman filtering algorithm in Section 3.2.1, since the road input displacement is one of the system state variables, the filtering estimation of the road excitation can be regarded as the filtering estimation of the vibration system.

3.3. Example Analysis of the Road Identification Model

According to the vehicle road surface identification principle of adaptive Kalman filter with forgetting factor, the test vehicle test system is established. The experimental vehicle used in this paper is the independent suspension modified by Volkswagen Longyi. The driving camera is set up to measure and record the vehicle's speed in real time. The body acceleration is observed by the acceleration sensor, and the relative displacement between the body and the suspension is observed by the displacement sensor. Finally, the data measured by the sensor is used as the observation value of the adaptive Kalman filtering algorithm with the forgetting factor, and the road input of the vehicle is filtered and estimated. The schematic diagram is shown in Figure 4.
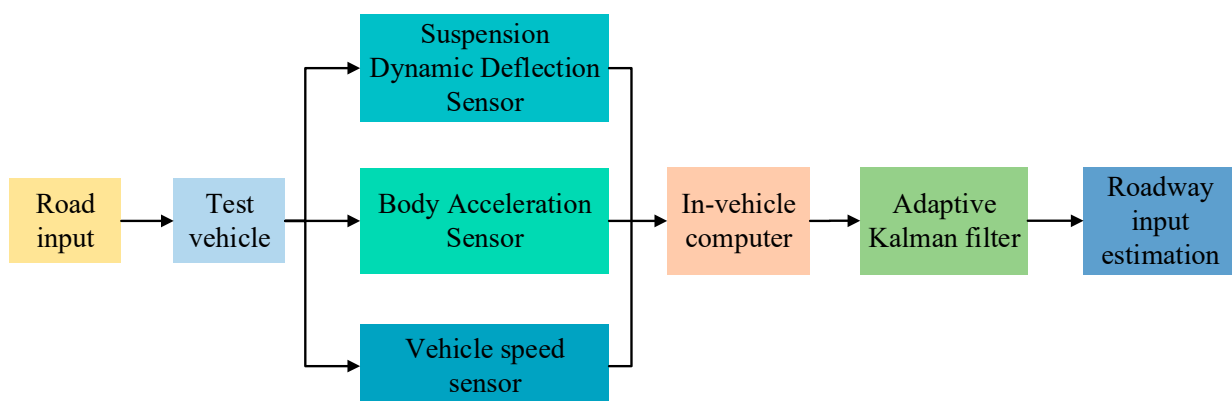

Figure 4. Schematic diagram of road surface recognition experiment.

The specific equipment installation scene, experimental equipment, and data acquisition device of the real vehicle road test are shown in Figure 5.
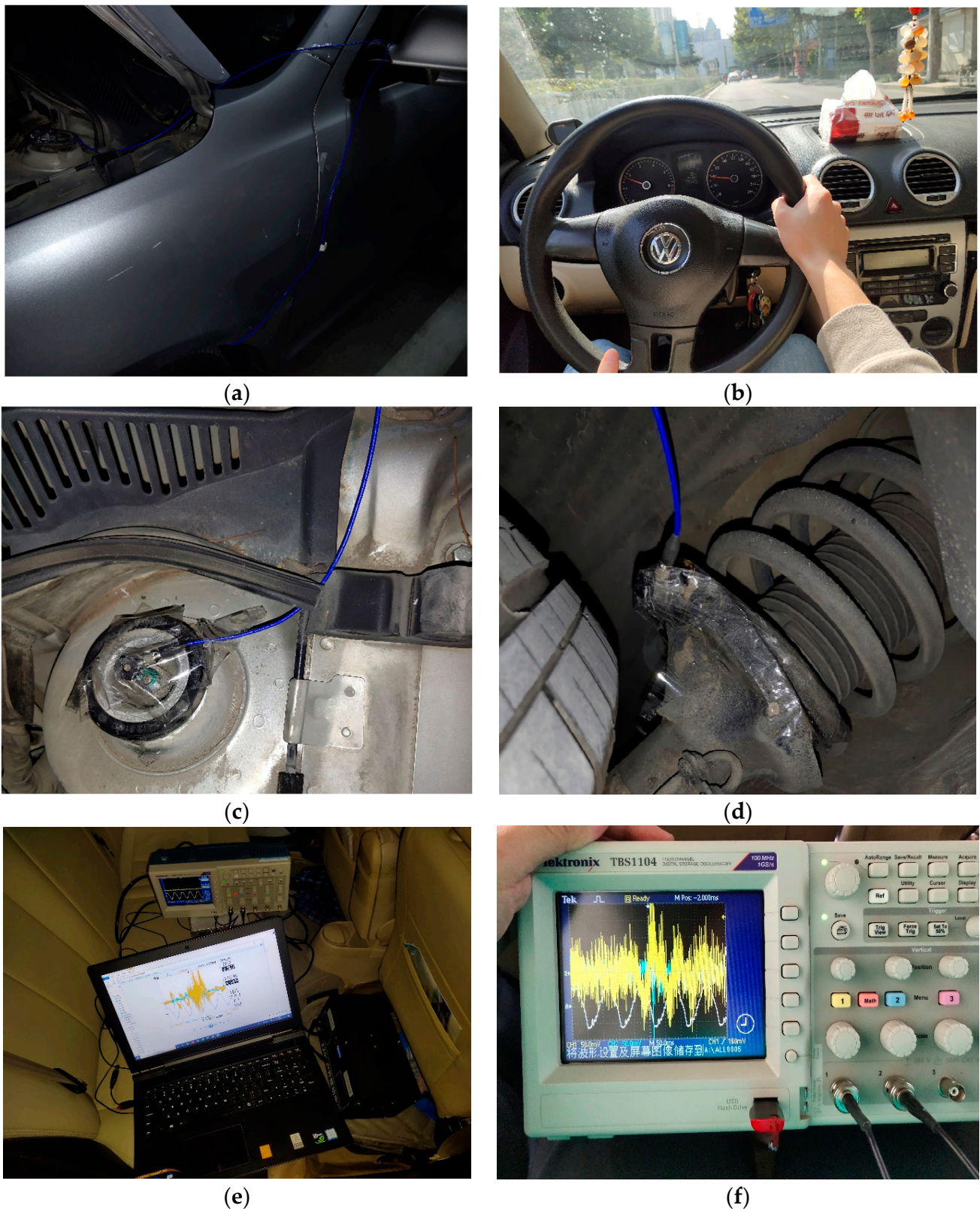
(**a**)

(**b**)

(**c**)

(**d**)

(**e**)

(**f**)

Figure 5. (**a**) Test vehicle exterior view. (**b**) Vehicle speed acquisition chart. (**c**) Body acceleration data acquisition. (**d**) Suspension dynamic deflection data acquisition. (**e**) Vibration response data acquisition. (**f**) Oscilloscope data acquisition.

According to the previous analysis of the road surface identification model, a 1/4 vehicle vibration system road surface estimation identification model is built into the software. The road estimation identification model takes the measured values of BA and SWS as the input data of road identification, and the optimal estimation of the road surface is obtained by the filtering calculation. In this paper, the road estimation identification model is simulated under the B-grade road conditions with the speed of 10 m/s and 20 m/s, respectively. The actual value of the road input is compared with the estimated value, and the simulation results are shown in Figures 6 and 7.
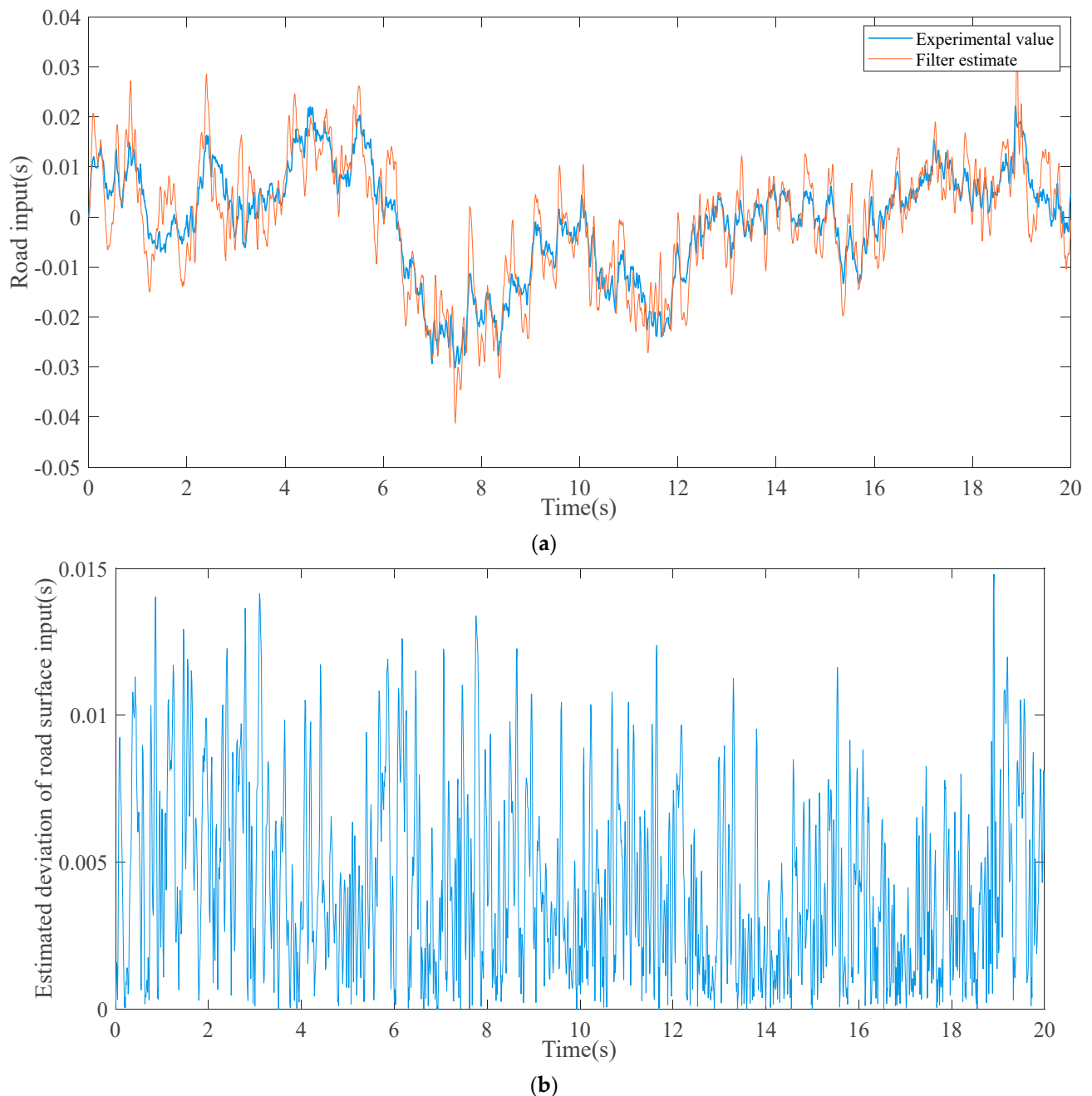

(a)

(b)

Figure 6. (**a**) The comparison between the experimental value and estimated value at 10 m/s. (**b**) Road input estimation bias at 10 m/s.
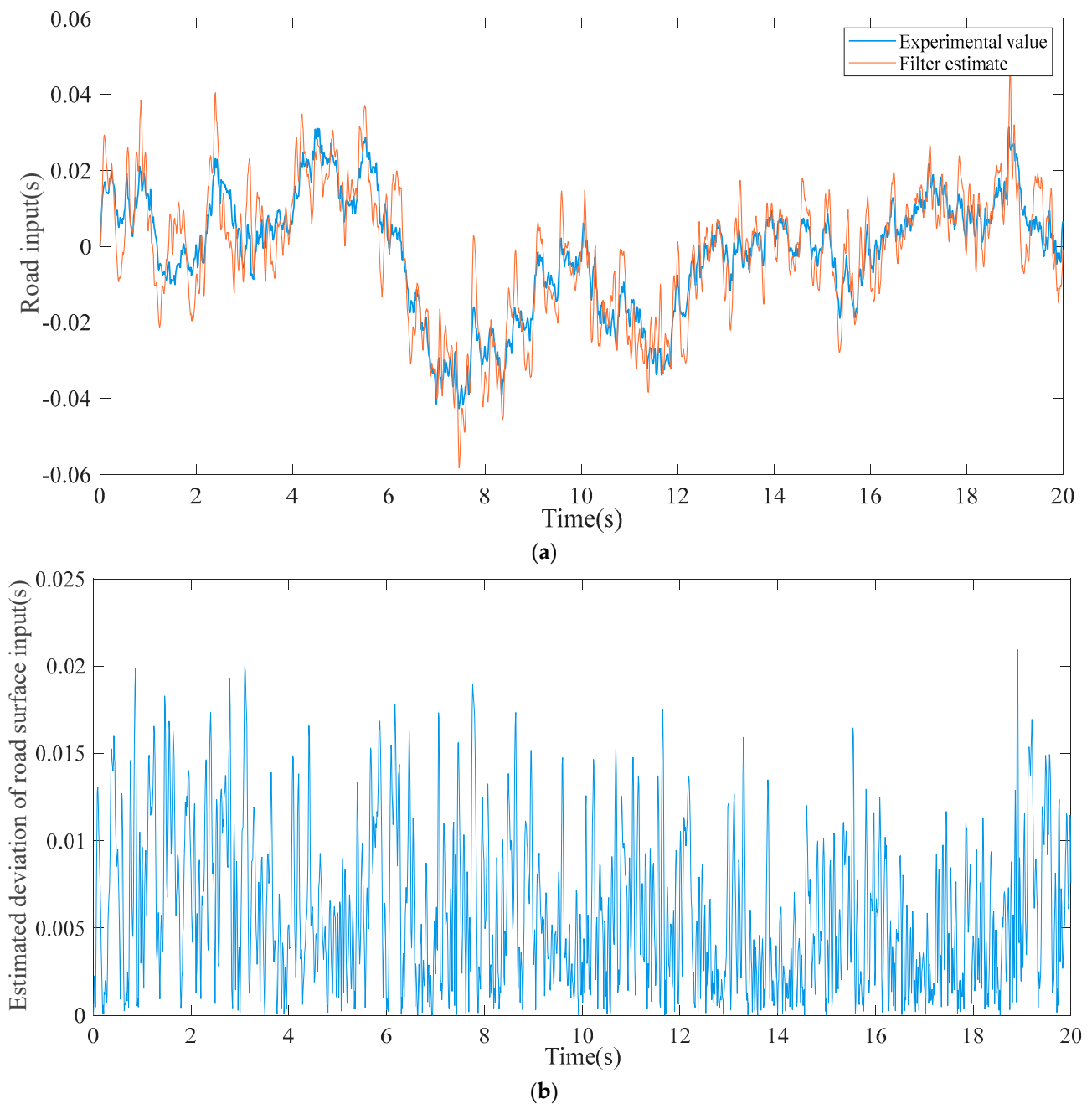
Figure 7. (**a**) The comparison between the experimental value and the estimated value at 20 m/s. (**b**) Road input estimation bias at 20 m/s.

It can be concluded from the figure that the two performance indicators of BA and SWS are used as input data, and the adaptive Kalman filter with forgetting factor is used to estimate the suspension vibration response parameters, and a more accurate filtering estimation result of road input displacement is obtained. Compared with the experimental value, the estimated value of the road input filter has no obvious phase difference and a small amplitude difference. After calculation, the mean values of the identification and estimation deviations of the vehicle road input are 0.0057 m and 0.0080 m, respectively, and the results of the road input estimation are more accurate. In this paper, road input estimation mainly refers to the change of the tire dynamic displacement during the driving process of the vehicle. Therefore, it provides a theoretical basis for the accurate switching of the working mode of the vehicle suspension vibration system in the fourth part and proves

that the accurate switching of the working mode can be completed by the tire dynamic displacement and the body acceleration.

4. Working Mode Switching Strategy Design

4.1. The Working Mode and Workflow of the Suspension System

The intelligent suspension system described in this paper can provide four working modes for drivers and passengers [23–25], as shown in Figure 8 below. The active control mode can improve the driving safety, driving smoothness, and handling stability of the vehicle. The regenerative working mode can recover and utilize the energy generated by the vibration of the vehicle suspension, which is beneficial to increase the mileage of the electric vehicle.
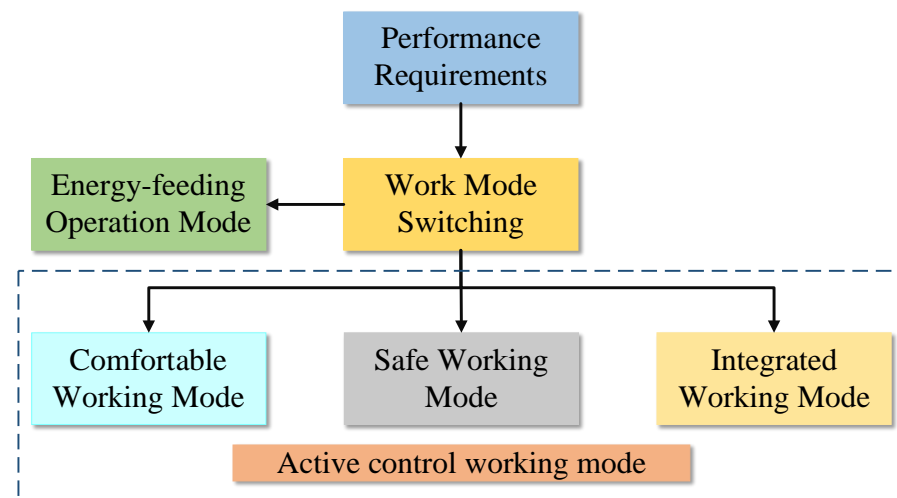

Figure 8. Sensor-based active suspension working mode.

The mode-switching control strategies for different roads are briefly introduced as follows:

(1)   Comfort working mode

Using the BP neural network (back propagation error) control and PID control algorithm, the vertical acceleration of the vehicle body is taken as the main optimization object to improve the ride comfort of the vehicle on the B-grade road.

(2)   Security working mode

Using the LQR algorithm (linear quadratic optimal control), the dynamic displacement of the wheel is taken as the main optimization object to improve the adhesion between the tire and the road surface, enhance the driving safety, and improve the ride comfort of the vehicle on the C-grade road surface.

(3)   Comprehensive working mode

The GA-LQR algorithm (Gaussian linear quadratic control optimized by genetic algorithm) is used to improve the driving safety, handling stability, and ride comfort of the vehicle, and improve the comprehensive performance of the vehicle on the D-grade road surface.

(4)   Energy feedback working mode

At this time, the DC motor acts as a generator to recover and store the energy generated by the active suspension vibration. When the vehicle is running on a good road, such as an A-grade road, the driver can choose the working mode independently, which is conducive to improving the mileage of the vehicle; in addition, it can also be used in other working modes, such as D-grade road surface, while selecting the energy-regenerative working mode to continuously recover electricity to increase the mileage of electric vehicles.

In the process of vehicle driving, due to the obvious changes in different road driving conditions, the driver's demand for vehicle performance also changes. The intelligent suspension system in this paper can provide users with a working mode suitable for driving on the current road surface and meet the needs of users for vehicle driving performance. The workflow diagram is shown in Figure 9.
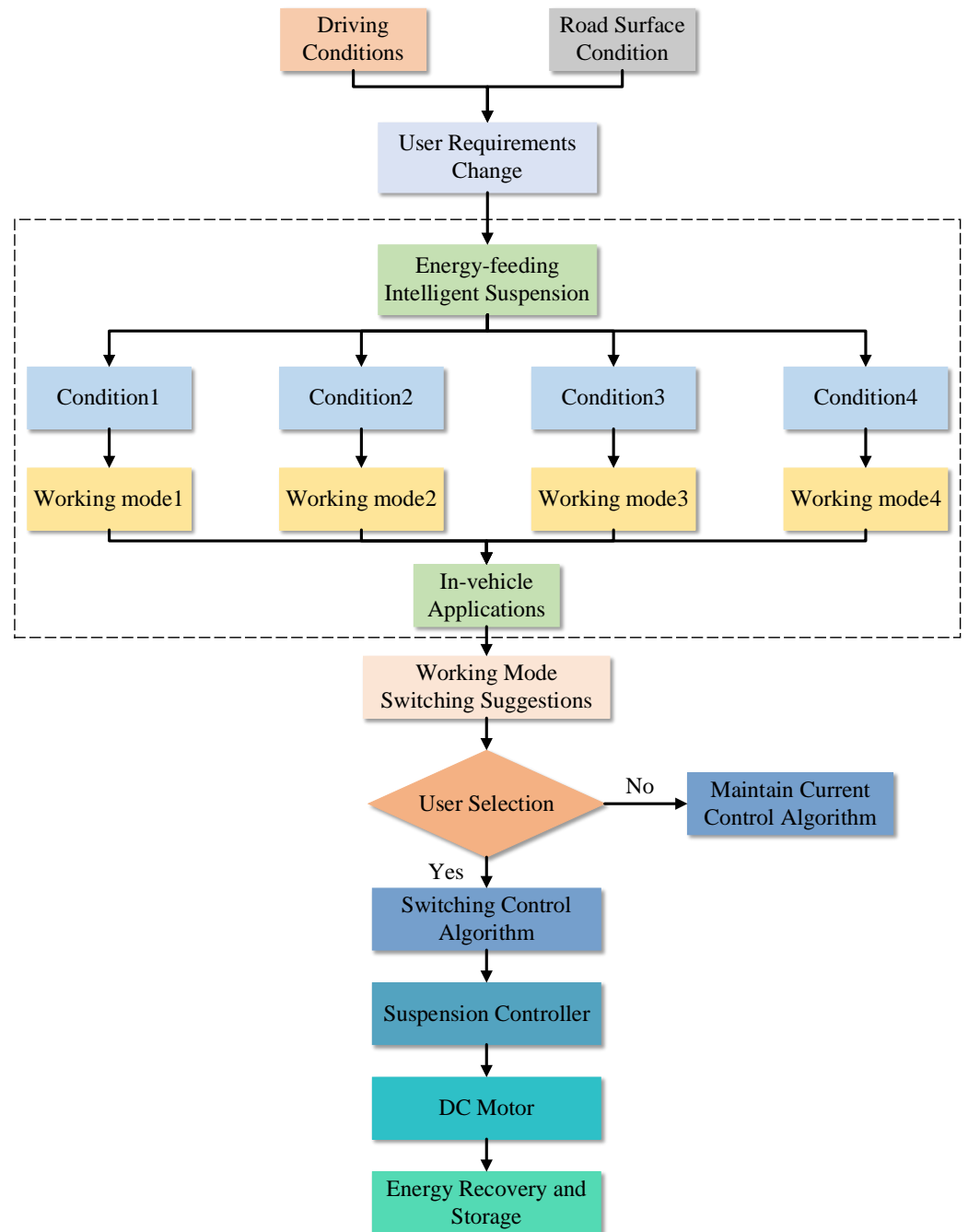

Figure 9. Suspension system workflow chart.

The flow chart of the suspension system mainly includes two parts. One is the software part of the intelligent suspension, including the working mode of the suspension system, the road input estimation algorithm, the corresponding control algorithm (marked with a dotted box), and the vehicle application program. The second is the hardware equipment, including the DC motor, ECU, energy storage device, actuator, suspension controller, etc. When the driving condition of the vehicle changes, the ECU processes the vibration

signal transmitted by the sensor through logical judgment rules and recommends the working mode matching the road driving condition to the driver through the onboard application. The user can switch the recommended working mode autonomously. When the user determines to switch the working mode, the suspension controller will control the DC motor to enter the corresponding working state. When the user chooses the energy-regenerative working mode, the DC motor works as a generator, and the electric energy generated by the vibration of the vehicle suspension is transmitted to the energy storage device through the control circuit, which can not only provide electric energy for other equipment in the car but also increase the cruising range of the car, especially the electric vehicle. When the user chooses the active control working mode, the DC motor works as the motor. Under the control of the optimization algorithm corresponding to each working mode, the system will output the active power suitable for the current road grade and improve the vehicle suspension performance required by the user.

4.2. Single-Double Threshold Sequential Judgment Switching Method

The active suspension system designed in this paper switches the corresponding four working modes according to the road grade A-D grade and divides the road grade D and above into the D-grade road. The main reason for this division is to consider that the common D-grade and above pavements are rare in common urban pavements. It is also to improve the accuracy of the division to a certain extent and avoid the complexity caused by excessive fine division.

Tire grip is directly reflected by tire dynamic displacement (DTD), which is the main evaluation index of vehicle driving safety. The ride comfort of the occupants is mainly reflected by the body acceleration (BA), which is an important evaluation index of vehicle ride comfort. Therefore, this paper takes these two evaluation indexes as the judgment criteria of working mode switching and achieves an accurate switching effect by setting corresponding thresholds.

In most cases, the safety of vehicle driving is more important than comfort. Therefore, when designing a single-double threshold sequential judgment strategy, the tire dynamic displacement and body acceleration are used as the first and second judgment criteria, respectively. The conclusion of the judgment strategy is which grade of the road the current road is. Based on the above judgment strategy, it is not only beneficial to ensure the driving safety of drivers and passengers, but also improves the efficiency of the judgment calculation.

The judgment strategy of the working mode of the intelligent suspension system is as follows:

(1) When $\forall \left(z_t - z_f \right) < \left(z_t - z_f \right)_1 \wedge \ddot{z}_s < \ddot{z}_{s1}, \exists RM = A$, the actual value of the tire dynamic displacement is less than the set threshold and the actual value of the body acceleration is less than the threshold, it is judged that the vehicle is driving on the A-grade road surface. At this time, the tire dynamic displacement and body acceleration are small, and the dynamic performance of the vehicle is good. The system will provide an energy-regenerative working mode for users to switch, and recover the energy generated by the vibration of the vehicle suspension.

(2) When $\forall \left(z_t - z_f \right) < \left(z_t - z_f \right)_1 \wedge \ddot{z}_s \geq \ddot{z}_{s1}, \exists RM = B$, it is judged that the vehicle is driving on the B-grade road. Due to the increase in body acceleration, the ride comfort of drivers and passengers becomes worse. The system will provide a comfortable working mode for users to switch, to improve the ride comfort of vehicles.

(3) When $\forall \left(z_t - z_f \right) \geq \left(z_t - z_f \right)_1 \wedge \ddot{z}_s \leq \ddot{z}_{s2}, \exists RM = C$, it is judged that the vehicle is driving on the C-grade road surface. Due to the increase in road roughness, the tire dynamic displacement gradually increases, and the tire grip is poor. The system will provide a safe working mode for users to switch to improve the driving safety of the vehicle.

(4) When $\forall \left(z_t - z_f \right) \geq \left(z_t - z_f \right)_1 \wedge \ddot{z}_s > \ddot{z}_{s2}, \exists RM = D$, it is judged that the vehicle is driving on the D-grade road. At this time, due to the increase in tire dynamic dis-

placement and body acceleration, the dynamic performance of the vehicle decreases. The system will provide a comprehensive working mode for users to switch and to optimize driving safety, handling stability, and ride comfort, and then improve the comprehensive performance of the vehicle. In addition, the driving speed of D-grade road vehicles is not high, and the energy generated by suspension vibration is high, which can provide users with the energy-regenerative working mode at the same time.

In summary, the suspension system working mode switching strategy table is listed, as shown in Table 2.

Table 2. Working mode switching strategy.

DTD	BA	Pavement Grade	Working Mode
$\left(z_t - z_f\right) < \left(z_t - z_f\right)_1$	$\ddot{z}_s < \ddot{z}_{s1}$	A	Feedthrough Mode
	$\ddot{z}_s \geq \ddot{z}_{s1}$	B	Comfort Mode
$\left(z_t - z_f\right) \geq \left(z_t - z_f\right)_1$	$\ddot{z}_s \leq \ddot{z}_{s2}$	C	Security Mode
	$\ddot{z}_s > \ddot{z}_{s2}$	D	Comprehensive Mode/ Feedthrough Mode

4.3. Working Mode Switching Threshold Setting

In most cases, the normal speed of the car is generally maintained in the speed range of 10–30 m/s. Through simulation, it can be seen that both DTD and BA are positively correlated with vehicle speed and road roughness, and road roughness has a greater impact on evaluation indicators. When the vehicle is driving on the A-grade road, both DTD and BA are smaller; when the vehicle is driving on the D-grade road, both DTD and BA are larger; when the vehicle runs at a speed of 10 m/s on the C-grade road, the two performance indicators of DTD and BA are greater than the vehicle running at a speed of 30 m/s on the B-grade road.

In summary, $\left(z_t - z_f\right)_1$ is the root mean square value $\left(z_t - z_f\right)_{B\max}$ of the dynamic displacement of the tire under the condition of the passive suspension on the B-grade road at a speed of 30 m/s; let $\ddot{z}_{s1}$ be the root mean square value $\left(\ddot{z}_s\right)_{B\min}$ of the body acceleration of the passive suspension under the condition of driving at 10 m/s on the B-grade road surface; let $\ddot{z}_{s2}$ be the root mean square value $\left(\ddot{z}_s\right)_{C\max}$ of the body acceleration of the passive suspension under the condition of 30 m/s speed driving on the C-grade road surface, as follows:

$$\left(z_t - z_f\right)_1 = \left(z_t - z_f\right)_{B\max} \tag{24}$$

$$\ddot{z}_{s1} = \left(\ddot{z}_s\right)_{B\min} \tag{25}$$

$$\ddot{z}_{s2} = \left(\ddot{z}_s\right)_{C\max} \tag{26}$$

The simulation results show that the thresholds are $\left(z_t - z_f\right)_1 = 8.7282 \times 10^{-4}$ m, $\ddot{z}_{s1} = 0.2812 \text{ m/s}^2$, $\ddot{z}_{s2} = 0.9205 \text{ m/s}^2$, respectively. Combined with the comparison of the estimation results of the road input using the adaptive Kalman filter algorithm in the third part, the intelligent suspension system can accurately and clearly distinguish the roads at all grades.

4.4. Working Mode Switching Control Process

When the driving condition of the vehicle changes, the sensor signals on the body and tires are processed by the analog-to-digital converter and transmitted to the ECU. The ECU performs logical judgment processing on the signal, calculates the current tire dynamic displacement (i.e., road input estimation) and the root mean square value of the body acceleration, and compares the results with the pre-set threshold. The system pushes the

determined working mode to the driver through the onboard application. After the user confirms the selection of the working mode, the system processes the signal through the digital-to-analog converter and transmits it to the suspension controller. Under the optimal control of the corresponding algorithm, the working mode is switched. The working mode switching control process is shown in Figure 10 below.
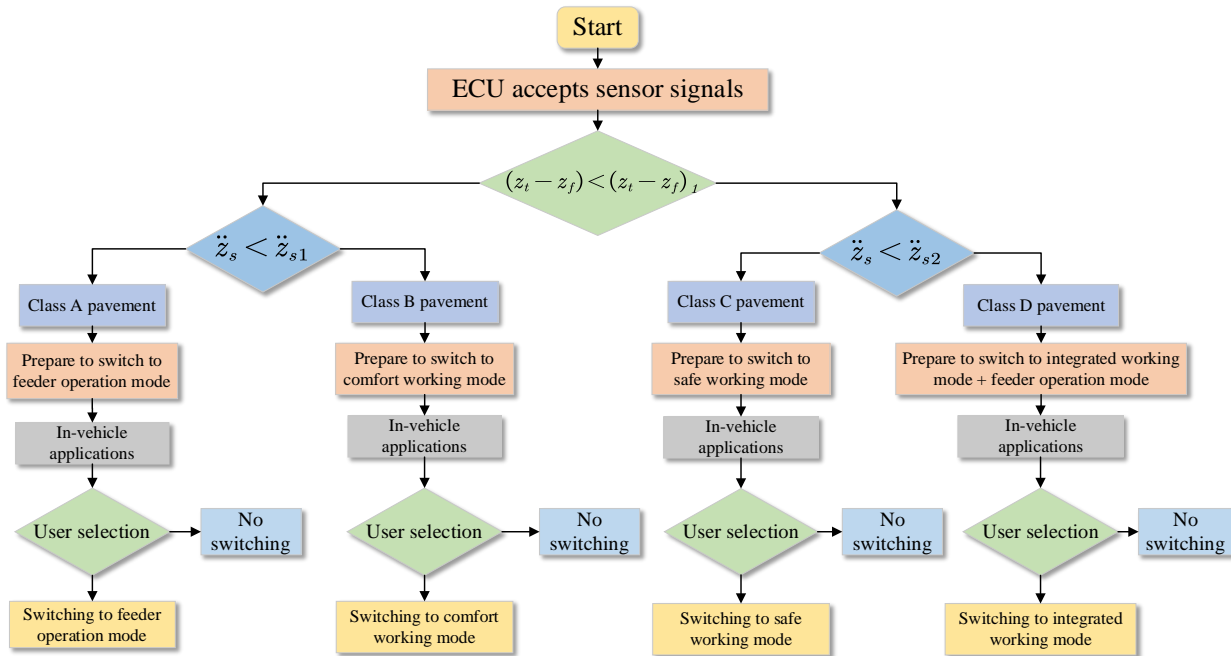

Figure 10. Working mode switching control process.

5. Design and Simulation Analysis of the Intelligent Suspension Controller Based on Sensor

In this paper, all working modes are simulated and analyzed by software. Due to the most frequent and lengthy driving of vehicles on B and D two-stage roads, the comfort and comprehensive working modes are mainly listed here. After establishing the road model and the vehicle system dynamics model, the fifth part will simulate and analyze the control algorithms corresponding to the system controllers under different working modes.

5.1. Vehicle Model Simulation Parameters

The parameters of the vehicle model come from a car, and the relevant parameters of the vehicle model are shown in Table 3 [26].

Table 3. Vehicle model simulation input parameters.

Parameter	Numerical Value
Body mass m_s/kg	320
Tire mass m_t/kg	40
Suspension spring stiffness $k_s/(N \cdot m^{-1})$	20,000
Suspension damping factor $c_s/(N \cdot s \cdot m^{-1})$	1000
Tire Stiffness $k_t/(N \cdot m^{-1})$	200,000
Vehicle speed $v_0/(m \cdot s^{-1})$	20
The lower limit cut-off frequency f_0/Hz	0.1

5.2. Optimization of the Comfort Working Mode Controller

Because the control law of state-based control algorithms, such as PID, is simple and easy to implement, and the parameters are easy to adjust, it is a control algorithm widely used in the control process. However, because the coefficients in the traditional PID control

are obtained through engineering experience and trial debugging, the long debugging process may cause functional damage to the controlled object; on the other hand, for the controlled object with nonlinear and time-varying characteristics, it is difficult to achieve the desired effect with the traditional PID controller.

In this paper, the PID control strategy and neural network control strategy are combined in the suspension controller to form a BP-PID composite algorithm [27–31], which is mainly used in the comfort working mode. BA is used as the primary optimization object to improve the ride comfort of the vehicle. Through software simulation, the results show that the controller designed by BP neural network method has better real-time performance and adaptability.

5.2.1. Structure and Algorithm of the BP-PID Controller

The BP-PID controller consists of a BP-neural network and PID controller. Firstly, the BP neural network adjusts the three parameters of the PID controller in real-time, and then the PID controller performs closed-loop control on the 1/4 vehicle model through the control force u, so that the system can obtain the best performance index. As shown in Figure 11, r is the expected output value of the system, y is the actual output value, e is the deviation between the two, K_p, K_i, and K_d are the proportional coefficient, integral coefficient, and differential coefficient that PID can achieve, and u is the output control force.
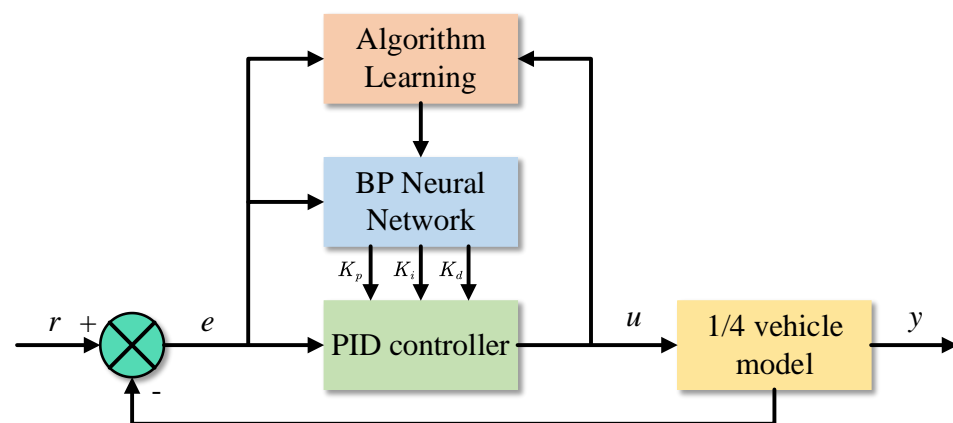

Figure 11. BP-PID controller structure diagram.

The BP neural network in this paper adopts a three-layer network structure, in which the number of neurons in the input layer is four, which is $x_1 = r(k)$, $x_2 = y(k)$, $x_3 = e(k)$, $x_4 = 1$, respectively, where $r(k)$, $y(k)$ is the expected output value and the actual output value of the system k, and $e(k)$ is the deviation between the two. The output value of the output layer neuron is the three parameters K_p, K_i, K_d of the PID controller, so the number of output layer nodes is three. The selection of the number of hidden layer nodes needs to be considered in two aspects. If the number of nodes is too large, the calculation amount of the BP neural network will be increased, resulting in too long self-learning time of the system. If the number of nodes is too small, the function approximation effect of the algorithm will become worse. In summary, this paper refers to the experience of existing scholars and determines the number of hidden layers nodes by trial-and-error method [32,33]. The goal is to ensure that the training accuracy and prediction accuracy of the network is the highest. The specific steps are:

(1) In the first trial, the number of neurons in the hidden layer is set to 1;

(2)　The network is trained by learning samples and tested by test samples after training. To describe the influence of the number of hidden layer neurons on the training accuracy and prediction accuracy, the following error expressions are used:

$$error = \frac{1}{2lp} \sum_{p=1}^{p} \sum_{j=0}^{l-1} (t_{jp} - y_{jp})^2 \tag{27}$$

where p is the number of samples; l is the number of neurons in the output layer; t is the model output; y is the sample output.

(3)　Increase the number of neurons in the hidden layer, repeat step (2), and observe the changes in the training error and prediction error of the network until the training error reaches the minimum and stabilizes, and the prediction error reaches the minimum.

(4)　The minimum number of hidden layer neurons with a small training error and the prediction error is taken as the number of hidden layer neurons in the model.

The BP neural network PID controller studied in this paper adopts a single hidden layer, and the number of hidden layers is 5. The BP neural network structure is shown in Figure 12, and the structure is 4-5-3.
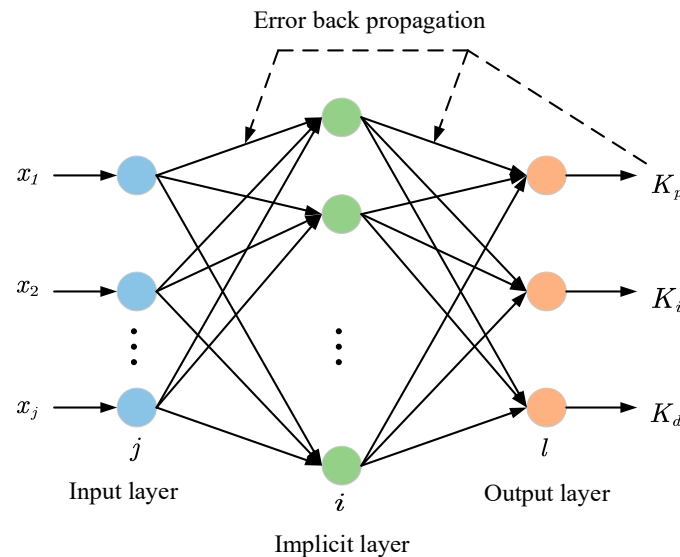

Figure 12. BP neural network structure diagram.

The BP-PID algorithm is introduced below.

The input of the input layer neuron is x_j, and the output $O_j^{(1)}$ is:

$$O_j^{(1)} = x_j (j = 1, 2, 3, 4) \tag{28}$$

The k-th input and output of the hidden layer neurons are:

$$\begin{cases} net_i^{(2)}(k) = \sum\limits_{j=1}^{4} w_{ij}^{(2)} O_j^{(1)} + \theta_i^{(2)} \\ O_i^{(2)}(k) = f\left[net_i^{(2)}(k) \right] \end{cases} (i = 1, 2, 3, 4, 5) \tag{29}$$

$$f(x) = \frac{e^x - e^{-x}}{e^x + e^{-x}} \tag{30}$$

In the formula, $w_{ij}^{(2)}$ and $\theta_i^{(2)}$ are the weights and thresholds of the hidden layer connection, respectively; $f(x)$ is a positive and negative symmetric Sigmoid function; the corner markers (1), (2), and (3) are respectively represented as the input layer, hidden layer, and output layer.

The *k*-th input and output of the network output layer neuron are:

$$\begin{cases} net_l{}^{(3)}(k) = \sum\limits_{i=1}^{5} w_{li}{}^{(3)} O_i{}^{(2)} + \theta_l{}^{(3)} \\ O_l{}^{(3)}(k) = g\left[net_l{}^{(3)}(k)\right] \end{cases} \quad (l = 1, 2, 3) \tag{31}$$

Among them:

$$\begin{cases} O_l{}^{(3)}(k) = K_p \\ O_2{}^{(3)}(k) = K_i \\ O_3{}^{(3)}(k) = K_d \end{cases} \tag{32}$$

$$g(x) = \frac{e^x}{e^x + e^{-x}} \tag{33}$$

where $w_{li}{}^{(3)}$ and $\theta_l{}^{(3)}$ are the connection weights and thresholds of the output layer, respectively; $g(x)$ is a nonnegative Sigmoid function.

The performance index function is:

$$E(k) = \frac{1}{2}[r(k) - y(k)]^2 \tag{34}$$

The gradient descent method with inertia term is used to modify the weights of the BP neural network so that $E(k)$ converges quickly to the negative gradient direction of weights.

$$w_{li}{}^{(3)}(k) = -\eta \frac{\partial E(k)}{\partial w_{li}{}^{(3)}(k)} + \alpha \Delta w_{li}{}^{(3)}(k-1) \tag{35}$$

$$\frac{\partial E(k)}{\partial w_{li}{}^{(3)}(k)} = \frac{\partial E(k)}{\partial y(k)} \cdot \frac{\partial y(k)}{\partial u(k)} \cdot \frac{\partial u(k)}{\partial O_l{}^{(3)}(k)} \cdot \frac{\partial O_l{}^{(3)}(k)}{\partial net_l{}^{(3)}(k)} \cdot \frac{\partial net_l{}^{(3)}(k)}{\partial w_{li}{}^{(3)}(k)} \tag{36}$$

$$\frac{\partial net_l{}^{(3)}(k)}{\partial w_{li}{}^{(3)}(k)} = O_i{}^{(2)}(k) \tag{37}$$

where $w_{li}{}^{(3)}(k)$ is the *k*-th connection weight of the output layer; $\Delta w_{li}{}^{(3)}(k)$ is the correction value of $w_{li}{}^{(3)}(k)$; $u(k)$ is the *k*-th output control force; η is the learning rate; α is the inertial coefficient.

Using the symbol function $\mathrm{sgn}[\partial y(k)/\partial u(k)]$ to approximate the unknown quantity $\partial y(k)/\partial u(k)$, the inaccuracy of the calculation is compensated by adjusting η. The following correction formulas for the weights and thresholds of the network output layer are listed:

$$\begin{cases} \Delta w_{li}{}^{(3)}(k) = \alpha \Delta w_{li}{}^{(3)}(k-1) + \eta \delta_l{}^{(3)} O_i{}^{(2)}(k) \\ \Delta \theta_l{}^{(3)}(k) = \alpha \Delta \theta_l{}^{(3)}(k-1) + \eta \delta_l{}^{(3)} \\ \delta_l{}^{(3)} = e(k) \cdot \mathrm{sgn}\left[\frac{\partial y(k)}{\partial u(k)}\right] \cdot \frac{\partial u(k)}{\partial O_l{}^{(3)}(k)} \cdot g'\left(net_l{}^{(3)}(k)\right) \end{cases} \tag{38}$$

where $\Delta \theta_i{}^{(2)}(k)$ is the correction value of the *k*-th threshold $\theta_i{}^{(2)}(k)$ of the output layer; $f'(x) = \left[1 - f^2(x)/2\right]$.

### 5.2.2. Simulation and Analysis of the Comfort Controller

To verify the reliability and effectiveness of the BP-PID controller designed above, this paper establishes a nonlinear suspension system control simulation model in the simulation software and simulates the performance of the passive suspension, and active suspension using a conventional PID controller and BP-PID controller, respectively. The parameters of the suspension model are shown in Table 3.

When the vehicle is driving on the B-grade road at a speed of 20 m/s, the dynamic response curves of the body vertical acceleration, suspension dynamic stroke, and tire dynamic displacement of the passive suspension and the active suspension under the
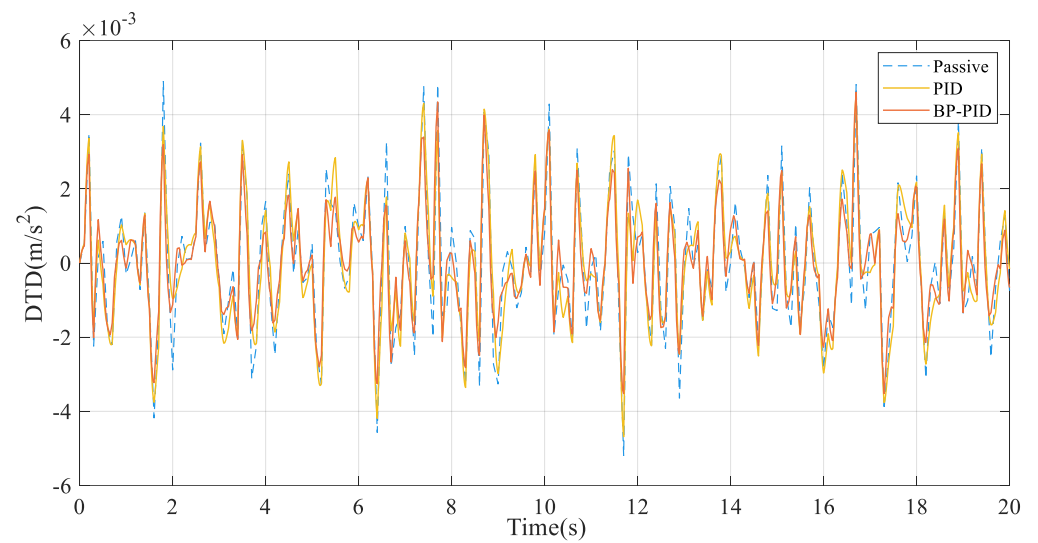
two controllers are shown in Figure 13. Through simulation calculation, $K_p = 0.9271$, $K_i = 0.9841$, and $K_d = 0.9796$ were finally obtained. The simulation experimental data are analyzed, and the comparison of the performance indexes of the active suspension and the passive suspension is obtained. The RMS values are listed in Table 4.
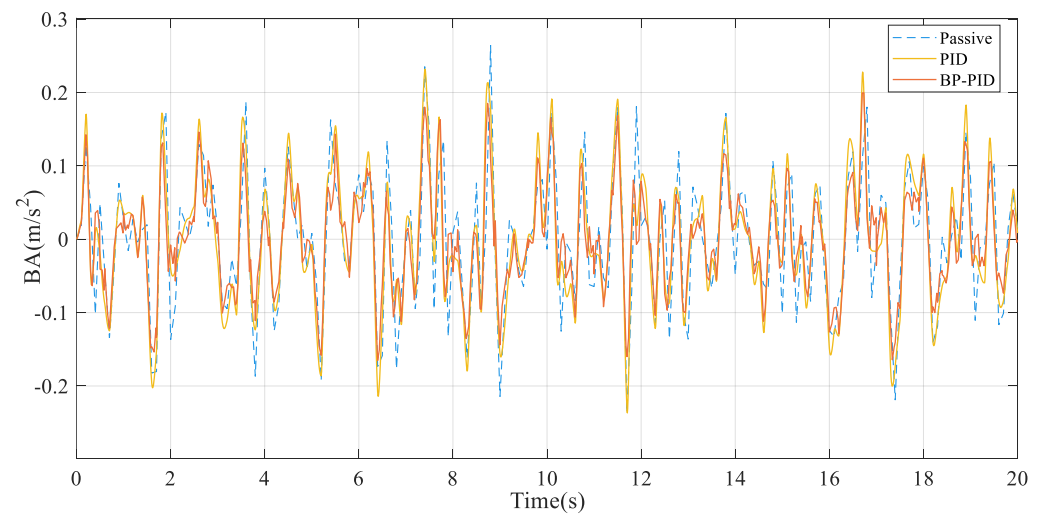
(**a**)
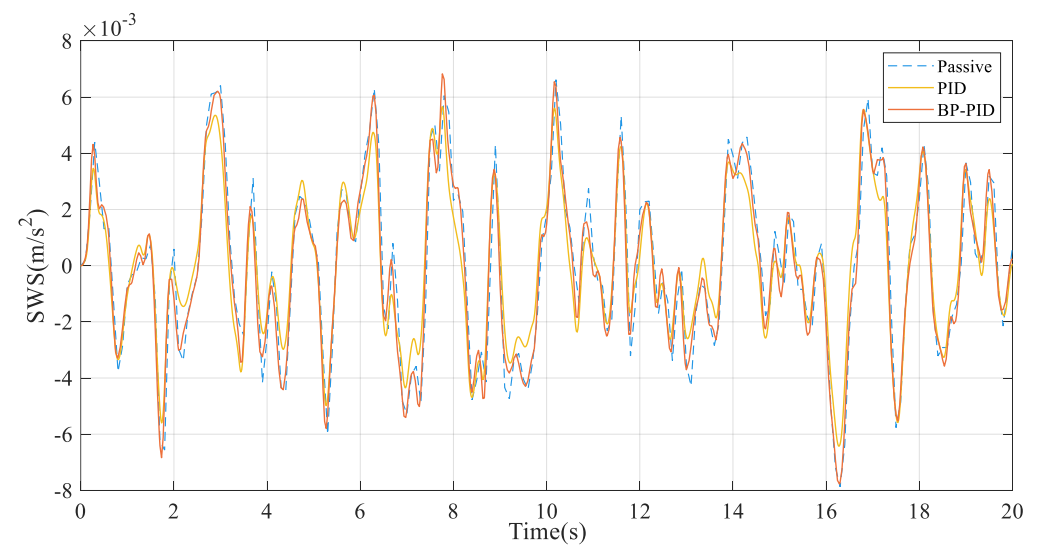
(**b**)

(**c**)

Figure 13. (**a**) Body acceleration curve; (**b**) suspension working space curve; and (**c**) tire dynamic displacement curve.

Table 4. Root mean square value of performance index.

Performance Indicators	Passive	PID	BP-PID
BA $/(\text{m} \cdot \text{s}^{-2})$	0.0927	0.0853	0.0688
SWS $/(\text{mm})$	3.1000	2.5000	2.9000
DTD/(mm)	1.9000	1.6000	1.4000

It can be seen intuitively from Figure 13 that the BA amplitude of the passive suspension vibrates in the range of $(-0.2 \text{ m/s}^2 – 0.3 \text{ m/s}^2)$ under the driving condition of 20 m/s on the B-grade road surface, while the BA amplitude of the active suspension controlled by BP-PID vibrates in the range of $(-0.1 \text{ m/s}^2 – 0.1 \text{ m/s}^2)$. It can be seen from Table 4 that compared with the passive suspension, the BA index of the active suspension optimized by the BP-PID algorithm is reduced by 26%, the DTD index is reduced by 27%, and the SWS index is reduced by 5%. From the comparison results, it can be seen that the active suspension optimized by the BP-PID algorithm can improve the stability of vehicle driving to a certain extent and effectively improve the stability of user driving.

Compared with the active suspension optimized by the traditional PID algorithm, the BA index of the active suspension optimized by the BP neural network algorithm is further reduced by 19%, the DTD index is reduced by 12%, and the SWS index is increased by 16%. Through the above data, it can be seen that the BP-PID algorithm can better control the active suspension and further improve the ride comfort of the user. Although the SWS index has increased, it is still within the allowable range. In summary, both algorithms can improve the ride comfort of users to a certain extent, and the active suspension using the BP-PID algorithm has a greater improvement than that using a single PID algorithm, which proves the superiority of the BP-PID algorithm. It is more suitable for vehicles to improve the ride comfort of users when driving on B-grade roads.

5.3. Optimization of Comprehensive Working Mode Controller

The key to the design of the LQR optimal controller is the design of a weighting coefficient matrix $\boldsymbol{Q}$ and $\boldsymbol{R}$, and there is no fixed analytical method. Generally, there is no rule to follow, and the trial-and-error method is usually used to determine the value of the weighting coefficient matrix. The limitation of this method is low efficiency, and it is not guaranteed that the obtained weight matrix can obtain the optimal control of the suspension system.

In this paper, the genetic algorithm is introduced to optimize the weighting coefficient of the traditional LQR control algorithm. Through the global search ability of the genetic algorithm, the weighting matrix is optimized with the performance index of the active suspension as the objective function, aiming at improving the design efficiency and performance of the LQR. For the comprehensive working mode, the body acceleration, suspension dynamic stroke, and tire dynamic displacement are all taken as the optimization objectives, and the GA-LQR algorithm is used to improve the ride comfort and safety of the vehicle [34–36].

5.3.1. Structure and Algorithm of GA-LQR Controller

The performance index function J of the integrated controller is the integral of the weighted sum of squares of the above three evaluation indexes in the time domain T, and its expression is:

$$J = \lim_{T \to \infty} \frac{1}{T} \int_0^T \left\{ q_1 \ddot{z}_s{}^2 + q_1 (z_s - z_t)^2 q_3 \left(z_t - z_f \right)^2 \right\} dt \tag{39}$$

where q_1, q_2, and q_3 are the weighting coefficients of each performance index, respectively.

According to the optimal control theory, the formula (39) is rewritten as follows:

$$J = \lim_{T \to \infty} \frac{1}{T} \int_0^T \left\{ \boldsymbol{X}^T \boldsymbol{Q} \boldsymbol{X} + \boldsymbol{U}^T \boldsymbol{R} \boldsymbol{U} + 2\boldsymbol{X}^T \boldsymbol{N} \boldsymbol{U} \right\} dt \tag{40}$$

where $\boldsymbol{Q}$ and $\boldsymbol{R}$ are the weighted matrix of state variables and control variables, respectively. $\boldsymbol{N}$ is the weight of the cross term.

From the lqr function in the simulation software, the optimal gain feedback matrix $\boldsymbol{K}$ is obtained, that is:

$$[K, S, E] = lqr(A, B, Q, R, N) \tag{41}$$

where S is the solution of Ricciati equation and E is the eigenvalue of the system.

According to the feedback state variable $\boldsymbol{X}(t)$, the optimal control force $\boldsymbol{U}(t)$ of the actuator at the t time can be obtained:

$$\boldsymbol{U}(t) = -\boldsymbol{K}\boldsymbol{X}(t) \tag{42}$$

5.3.2. Optimization of LQR Weighting Coefficient by the Genetic Algorithm

A genetic algorithm is an efficient parallel global optimization search algorithm based on natural selection and genetics. It has been successfully applied in many fields, such as function optimization, intelligent control, pattern recognition, and combinatorial optimization. Using a genetic algorithm to optimize the LQR control weighting coefficient can obtain better optimal control.

The optimization process of the weighting coefficients q_1, q_2, and q_3 of the LQR controller based on the genetic algorithm is shown in Figure 14. The specific steps are as follows:

(1) The initial population of weighted coefficients q_1, q_2, and q_3 are generated, and the individual values are encoded in real numbers.

(2) Individuals are assigned to q_1, q_2, and q_3 in turn. According to the LQR control algorithm, the control feedback matrix $\boldsymbol{K}$ is obtained, and then the $\boldsymbol{K}$ is substituted into the formula (42) to obtain the optimal control force $\boldsymbol{U}(t)$, which is applied to the suspension model to obtain the root mean square value of the three performance indexes.

(3) Due to the different orders of magnitude and units of the three performance indexes of the active suspension, to normalize the comparison, the following performance indexes are used as the fitness function of the genetic algorithm, that is:

$$\min f(x) = \sum_{i=1}^3 \frac{\mathrm{RMS}[\Delta_i(q)]}{\mathrm{RMS}[\Delta_{ip}(q)]} \tag{43}$$

Constraint conditions:

$$\mathrm{s.t.RMS}[\Delta_i(q)] < \mathrm{RMS}[\Delta_{ip}(q)] i = 1, 2, 3 \tag{44}$$

where RMS is the root mean square value of the three performance indexes of the suspension; $\Delta_i(q)$ is the performance index of active suspension; the following table p refers to passive suspension; and $q = [q_1, q_2, q_3]$ denotes the weighted coefficient vector.

Under the premise of satisfying the constraint condition (50), the minimum value of the fitness function is taken as the termination condition of the genetic algorithm program. According to the Formula (49), the fitness function value of the genetic algorithm is obtained to determine whether the termination condition is satisfied. If satisfied, the genetic algorithm is withdrawn, and the optimal individual value is returned. Otherwise, go to step (4).

(4) If the genetic algorithm continues to select, cross, mutate, go to the execution step (2), generate a new population, re-circulate, and exit the cycle until the termination conditions are met.
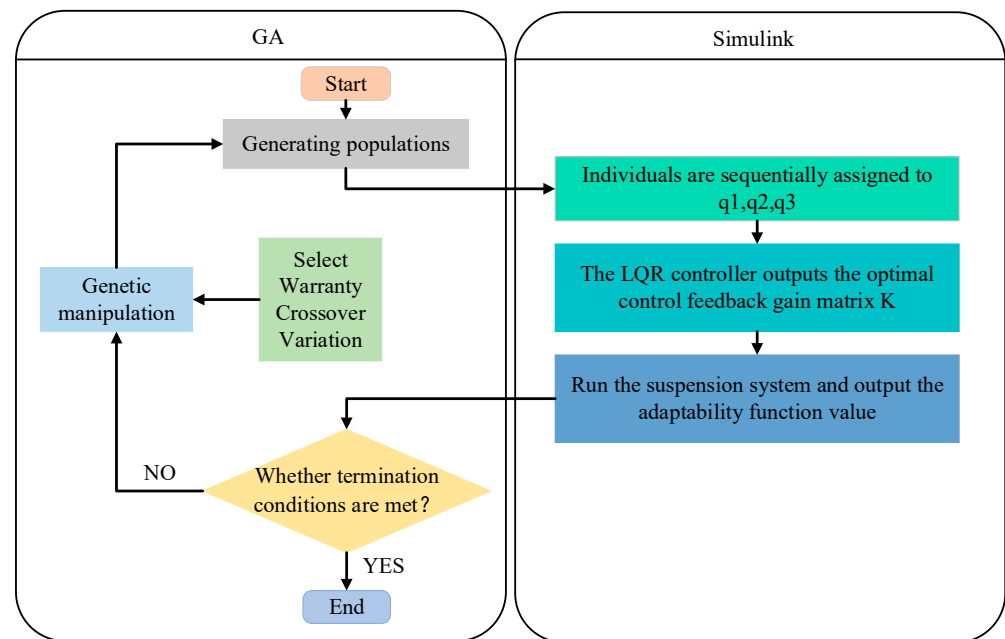
Figure 14. Genetic algorithm optimization design LQR controller diagram.

5.3.3. Optimization of LQR Weighting Coefficient by the Genetic Algorithm

To verify the reliability and effectiveness of the above-designed GA-LQR controller, a nonlinear suspension system control simulation model is established in the simulation software. The performance of the passive suspension, active suspension using conventional LQR controller, and GA-LQR controller is simulated and analyzed. The parameters of the suspension model are shown in Table 3.

When the vehicle is driving on the D-grade road at a speed of 20 m/s, the dynamic response curves of the body vertical acceleration, suspension dynamic stroke, and tire dynamic displacement of the passive suspension and the active suspension under the two controllers are shown in Figure 15. Through simulation calculation, K = [1401.174, 968.1317, −11076.3, 18279.97, −5842.11] is finally obtained. The simulation experimental data are analyzed, and the comparison of the performance indexes of the active suspension and the passive suspension is obtained. The RMS values are listed in Table 5.

Table 5. Root mean square value of performance index.

Performance Indicators	Passive	LQR	GA-LQR
BA/$(\text{m} \cdot \text{s}^{-2})$	1.6725	0.9696	1.0289
SWS/(mm)	24.8000	22.4000	19.4000
DTD/(mm)	2.8000	2.4000	2.2000

It can be intuitively seen from Figure 15 that under the driving condition of a D-grade road speed of 20 m/s, the amplitude of BA and DTD of passive suspension vibrates in the range of (−4 m/s²–4 m/s²) and (−0.005 m–0.007 m), respectively, while the amplitude of BA and DTD of active suspension controlled by GA-LQR vibrates in the range of (−2 m/s²–2 m/s²) and (−0.004 m–0.005 m), respectively. According to Table 5, compared with the passive suspension, the BA index of the active suspension optimized by the GA-LQR algorithm is reduced by 38%, the DTD index is reduced by 24%, and the SWS index is reduced by 22%. From the comparison results, it can be seen that the active suspension optimized by the GA-LQR algorithm can effectively improve the user's ride comfort and driving stability, improve the comprehensive performance of the car, and effectively reduce the suspension breakdown probability so that the suspension workspace is fully utilized.
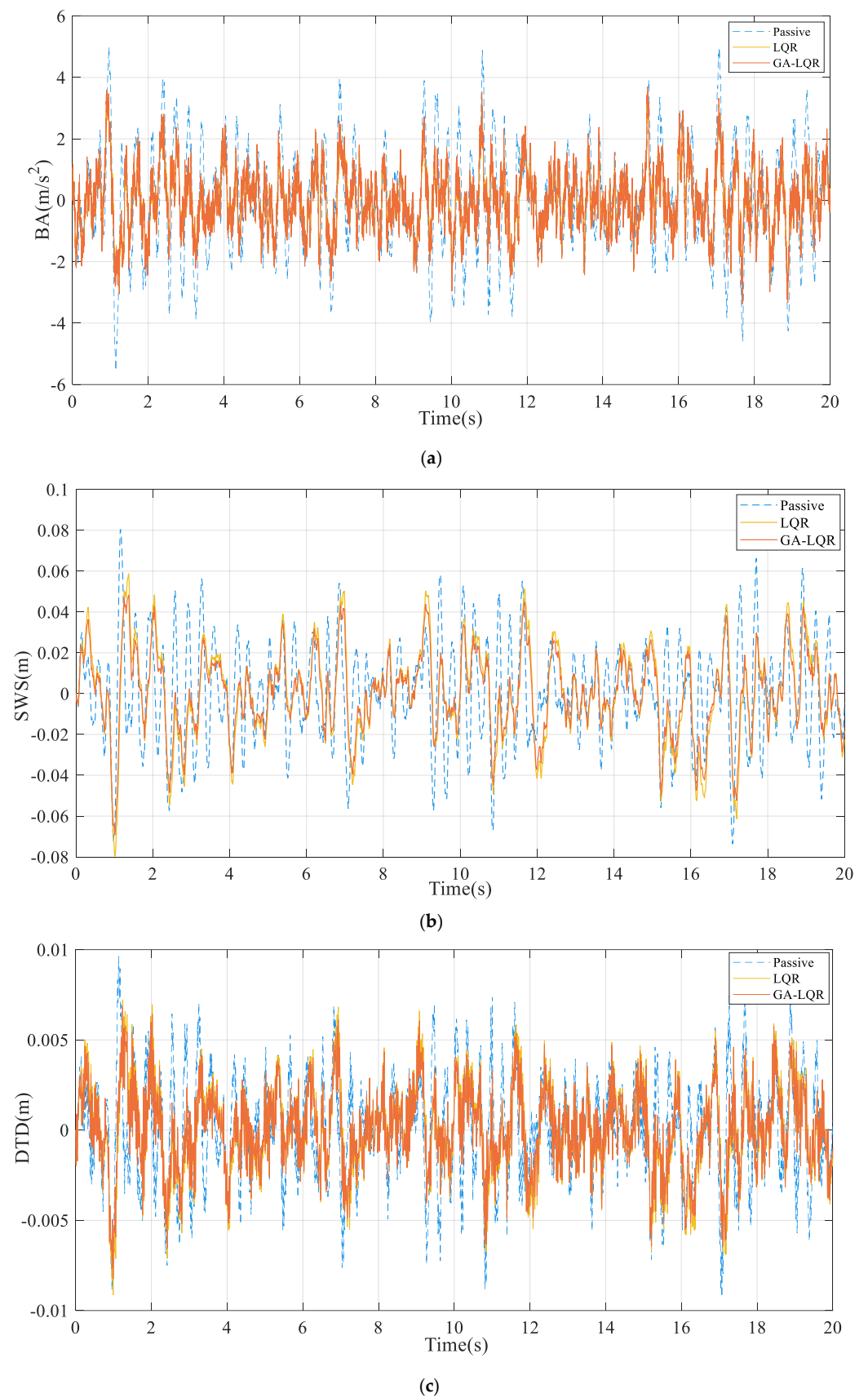
(**a**)

(**b**)

(**c**)

Figure 15. (**a**) Body acceleration curve; (**b**) suspension working space curve; and (**c**) tire dynamic displacement curve.

Compared with the active suspension optimized by the traditional LQR algorithm, the SWS index of the active suspension optimized by the genetic algorithm is further reduced by 9%, the DTD index is reduced by 14%, and the BA index is increased by 6%. Through the above data, it can be seen that the GA-LQR algorithm can better control the active suspension so that the user's ride comfort is further improved. Although the BA index has increased, it is still within the allowable range, and it also reflects that there is a certain contradiction between improving the ride comfort and handling stability of the vehicle at the same time. In summary, both algorithms can improve the comprehensive performance of automobile driving to a certain extent, and the active suspension using the GA-LQR algorithm has a greater improvement than that using a single LQR algorithm, which proves the superiority of the GA-LQR algorithm. It is more suitable for vehicles to improve the comprehensive performance of automobile driving on D-grade roads.

6. Conclusions

To meet the driver's different needs for vehicle performance when driving under different road conditions and respect the driver's independent choice, this paper proposes a sensor-based intelligent suspension system and studies its structural framework, working mode, and switching strategy. The design and simulation of the underlying controller are studied. The main conclusions are as follows:

(1) In this paper, in the process of determining the road grade, the filter estimator of the active suspension system is improved by the adaptive Kalman filter algorithm with a forgetting factor. The road input estimation results of the vehicle at the speed of 10 m/s and 20 m/s on the B-grade road surface are simulated and verified. It is concluded that there is no obvious phase difference between the estimated value of the road input filter and the real value, and the amplitude of the measurement result is small. The root mean square values of the estimated value and the experimental value of the road input estimation deviation are 0.0057 m and 0.0080 m, respectively, and the estimation results are more accurate.

(2) To increase the driver's flexibility and selectivity to the working mode, this paper introduces the user decision-making link. In the aspect of working mode switching, a mode-switching strategy based on a single-double threshold is designed. The strategy includes two decision-making links, which clarify the principle of limited safety. In the setting of the working mode switching threshold, the A-D road surface is accurately identified by the adaptive Kalman filter estimator, and the intelligent switching of energy feedback, comfort, safety, and comprehensive working mode is quickly realized.

(3) In this paper, in the comfort working mode, to solve the problem that the coefficients in the traditional PID controller are difficult to select and can only be obtained by engineering experience and trial and error debugging, the PID control strategy is combined with the neural network control strategy to form a BP-PID composite controller. Through simulation analysis, it can be seen that after using the BP-PID controller, the root means square values of the three indexes of BA, SWS, and DTD of the vehicle suspension are reduced by 26%, 5%, and 27%, respectively, compared with the passive suspension. Compared with the traditional PID control, the BA and DTD performance indexes of the active suspension are reduced by 19% and 12%, respectively, which effectively improves the ride comfort of the vehicle and the comfort of the user. It is found that with the deterioration of the road surface, the optimization degree of the three performance indexes of the suspension decreases, indicating that from the perspective of suspension control, the BP-PID composite control algorithm is more suitable for the vehicle to optimize and improve the vehicle performance when driving on the B-grade road surface, especially for the optimization of the BA performance index. It is more significant, which is conducive to improving the smoothness of the car during driving and improving the user's ride comfort.

(4) In the comprehensive working mode, the conventional LQR controller is easily affected by the designer's design experience. In this paper, the global search ability of the genetic algorithm is used to optimize the weight coefficient of the performance index in the LQR controller, and an LQR controller based on the genetic algorithm is proposed. Through simulation analysis, it can be seen that after using the GA-LQR controller, the root means square values of BA, SWS, and DTD of automobile suspension are reduced by more than 35%, 22%, and 20%, respectively, compared with passive suspension. Compared with the traditional LQR control, the active suspension SWS index is further reduced by 9%, the DTD index is reduced by 14%, and the BA index is increased by 6%, but it is still within the allowable range, which also reflects that there is a certain contradiction between improving the ride comfort and handling stability of the vehicle. Through the above simulation results, it can be seen that the GA-LQR composite control algorithm can better improve the ride comfort and handling stability of the vehicle, better solve the problem of selecting the weighting coefficient in the conventional LQR controller, and realize the optimal control of the suspension so that the vehicle can effectively improve the comprehensive performance of the vehicle when driving on the D-grade road surface and above the D-grade road surface.

References

1. Han, C.; Xu, L.; Zou, J. The research and verification of In-Arm Torsional Electromagnetic Active Suspension. *Proc. Inst. Mech. Eng. Part D J. Automob. Eng.* **2021**, *235*, 1379–1395. [CrossRef]
2. Liu, L.M. Research and simulation of optimal control of automobile semi-active suspension. *Mod. Inf. Technol.* **2022**, *6*, 132–135.
3. An, X.; Yang, Z.; Wang, Y. Multi-mode Dynamic Proportional Energy Management Strategy for Battery-Supercapacitor Hybrid Energy Storage System of Tram Based on Pseudo-spectrum Method. In Proceedings of the 2019 IEEE Transportation Electrification Conference and Expo, Asia-Pacific (ITEC Asia-Pacific), Seogwipo, Republic of Korea, 8–10 May 2019.
4. Tang, S.C.; Chen, L.; Wang, R.C. Research on the optimal control of active suspension based on damping multi-mode switching. *J. Guangxi Univ. Nat. Sci. Ed.* **2014**, *39*, 300–307.
5. Wang, R.C.; Ma, X.W.; Ding, R.K. Research on multi-mode switching control of hybrid suspension based on model reference. *J. Agric. Mach.* **2017**, *48*, 353–360.
6. Liu, Q.; Sun, J.W.; Zhang, H. Convolutional neural network-based road surface identification and semi-active suspension control. *J. Mil. Eng.* **2020**, *41*, 1483–1493.
7. Frej, G.; Moreau, X.; Hamrouni, E. Multi-Modes Control for Semi-Active Suspension Systems. *IFAC-Pap.* **2020**, *53*, 14407–14412. [CrossRef]
8. Ding, R.K. Research on energy-saving mechanism and intelligent switching control of hybrid electromagnetic active suspension for all-road conditions. *Jiangsu Univ.* **2020**, *10*, 27170.
9. Nguyen, L.H.; Hong, K.S.; Park, S. Road-frequency adaptive control for semi-active suspension systems. *Int. J. Control Autom. Syst.* **2010**, *8*, 1029–1038. [CrossRef]

10. Hassanzadeh, I.; Alizadeh, G.; Shirjoposht, N.P. A new optimal nonlinear approach to half car active suspension control. *Int. J. Eng. Technol.* **2010**, *2*, 78. [CrossRef]

11. Zhong, X.W.; Chen, S.; Zhang, B.Y. Research on vehicle vibration state estimation and optimal control based on Kalman filter algorithm. *Automot. Technol.* **2017**, *5*, 14–18.

12. Lu, F.; Chen, S.Z.; Liu, C.; Li, M.H.; Zhao, Y.Z. Vehicle vibration velocity estimation based on Kalman filter. *Vib. Shock* **2014**, *33*, 111–116.

13. Liu, Z.; Ren, H.; Chen, S. Feedback linearization Kalman observer based sliding mode control for semi-active suspension systems. *IEEE Access* **2020**, *8*, 71721–71738. [CrossRef]

14. Wang, R.C.; Wang, Y.J.; Ding, R.K.; Sun, D. Semi-active control of magnetorheological suspension based on Kalman observer. *J. Huazhong Univ. Sci. Technol. Nat. Sci. Ed.* **2020**, *48*, 49–54.

15. Wang, Z.F.; Dong, M.M.; Qin, Y.C.; Du, Y.C.; Zhao, F.; Gu, L. Suspension System State Estimation Using Adaptive Kalman Filtering Based on Road Classification. *Veh. Syst. Dyn.* **2017**, *3*, 371–398. [CrossRef]

16. Fan, Y.; Ren, H.; Chen, S. Observer design based on nonlinear suspension model with unscented kalman filter. *J. Vibroeng.* **2015**, *17*, 3844–3855.

17. Li, X.J. *Study on Intelligent Suspension Control Algorithm*; Qingdao University of Technology: Qingdao, China, 2019.

18. Wang, X.C. *Design of Machine Learning Database for LQG Active Suspension*; Qingdao University of Technology: Qingdao, China, 2020.

19. Liu, J.; Zhang, X. Transmission and energy-harvesting study for a novel active suspension with simplified 2-DOF multi-link mechanism. *Mech. Mach. Theory* **2021**, *160*, 104286. [CrossRef]

20. Wu, B.A.; Long, O.; Li, Y.G.; Ji, H.C.; Hui, X.W.; Zheng, Z. Optimal control of magnetorheological semi-active suspension based on genetic algorithm. *Mach. Tools Hydraul.* **2021**, *49*, 109–114.

21. Zhang, Q.; Zhang, L. Stability Analysis of the Kalman Predictor. *Int. J. Control* **2021**, *94*, 1217–1224. [CrossRef]

22. Wang, Y.Q. *Research on Estimation of Automotive State Parameters Based on Multi-Model Interaction Dual Extended Kalman Filter*; Shenzhen University: Shenzhen, China, 2020.

23. Meng, X.; Ding, R.; Sun, Z. Multi-mode switching control of hybrid electromagnetic suspension based on road conditions adaptation. *J. Theor. Appl. Mech.* **2020**, *58*, 697–710. [CrossRef]

24. Deng, Z.; Shi, B.; Wei, D. Research on Energy Reclaiming Active Suspension Control Strategy Based on Linear Motor and Hydraulic Hybrid System. *J. Phys. Conf. Ser.* **2021**, *1910*, 012041. [CrossRef]

25. Ma, X.W. *Design and Experimental Research on Multi-Mode Switching Control System for Hybrid Suspension*; Jiangsu University: Zhenjiang, China, 2017.

26. Yu, F.; Lin, Y. *Automobile System Dynamics, Version 2*; China Machine Press: Beijing, China, 2017.

27. Sabery, S.M.; Bystrov, A.; Gardner, P. Road Surface Classification Based on Radar Imaging Using Convolutional Neural Network. *IEEE Sens. J.* **2021**, *21*, 18725–18732. [CrossRef]

28. Sun, J.; Cong, J. Deep learning based road recognition for intelligent suspension systems. *Pol. Tow. Mech. Teor. I Stosow. (PTMTS)* **2021**. [CrossRef]

29. Liu, J.; Li, X.; Zhang, X. Modeling and Simulation of Energy-Regenerative Active Suspension Based on BP Neural Network PID Control. *Shock Vib.* **2019**, *2019*, 4609754. [CrossRef]

30. Wu, J.; Sun, X.; Wang, D. Model predictive direct suspension force control of a bearingless induction motor based on sliding mode observer. *Eng. Comput.* **2022**, *39*, 457–476. [CrossRef]

31. Cheng, Z.Y.; Yang, M.; Wu, X.J. Simulation analysis of active suspension based on BP neural network PID control. *Agric. Equip. Veh. Eng.* **2022**, *60*, 130–134.

32. Zhao, W.H. Research on PID Control Based on Neural Network Parameter Optimization. Ph.D. Thesis, North University of China, Taiyuan, China, 2008.

33. Liu, Y.M. Research on PID control method based on improved BP neural network. *Comput. Simul.* **2006**, *23*, 156–159.

34. Li, X.W.; Liu, J.; Teng, Y. LQG Active Control for Energy-Regenerative Suspension. *Mach. Des. Manuf.* **2018**, *6*, 90–93.

35. Chen, D.P.; Zhu, J.J.; Huang, Y.T.; Huang, M. Optimization simulation study of LQG algorithm for automotive active suspension. *Comput. Simul.* **2021**, *38*, 72–77.

36. Chen, L.J. Design of LQG controller for automotive active suspension based on genetic algorithm. *J. Xiamen Inst. Technol.* **2017**, *25*, 12–16.